Theoretical Comparison of Low and High Splitting Ratio Resonators

Raymond Carroll

The Charles Stark Draper Laboratory

555 Technology Square

Cambridge, MA 02139

tel: (617) 258-4508 fax: 258-1181

Robert Dahlgren

Fujikura Technology America Corp.

3001 Oakmead Village Dr.

Santa Clara CA 95051

tel: (408) 988-7407 fax: 727-3460

ABSTRACT

There are two possible topologies to fabricate fiber optic resonators which contain a single, low-loss coupler. The first resonators reported in the literature were of the spliceless design and required a high splitting ratio coupler; they are denoted as a cross-coupled fiber resonator (CFR). The development of low-loss splicing technology enabled rings to be constructed from low splitting ratio couplers, which have been referred to as direct coupled resonators (DFR) in the literature. In this paper, DFR and CFR will be theoretically compared, using a matrix formalism implemented in Mathematica™. Effects of a non optimum splitting ratio, differential normal mode losses, polarization cross-coupling, and backscatter will be examined. An optimum RFOG topology is suggested by this analysis.

COVER PAGE

THEORETICAL COMPARISON OF LOW- AND HIGH-SPLITTING RATIO RESONATORS

Raymond Carroll

The Charles Stark Draper Laboratory
555 Technology Square, Cambridge, MA 02139

Robert Dahlgren

Fujikura Technology American Corporation
3001 Oakmead Village Drive, Santa Clara, CA 95051

ABSTRACT

There are two possible topologies to fabricate fiber optic resonators which contain a single, low-loss coupler. The first resonators reported in the literature were of the spliceless design and required a high splitting ratio coupler; they are denoted as a cross-coupled fiber resonator (CFR). The development of low-loss splicing technology enabled rings to be constructed from low splitting ratio couplers, which have been referred to as direct coupled resonators (DFR) in the literature. In this paper, DFR and CFR will be theoretically compared, using a matrix formalism implemented in Mathematica™. Effects of a non optimum splitting ratio, differential normal mode losses, polarization cross-coupling, and backscatter will be examined. An optimum RFOG topology is suggested by this analysis.

1. SINGLE-MODE COUPLER THEORY

Figure 1 shows a block diagram representing a 2×2 single-mode coupler, with input fields labeled E_1 and E_2, and output fields E_3 and E_4. The two waveguides, represented by the dashed lines, are assumed to be parallel and of length L. The fields in waveguides A and B at any point z within $0 < z < L$ are expressed by a 2×1 column vector.
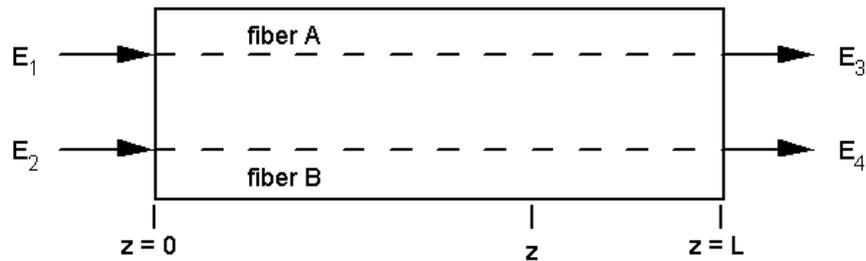

Figure 1. 2×2 Coupler Block Diagram.

$$E(z) \;=\; \begin{bmatrix} E_A(z) \\ E_B(z) \end{bmatrix} \qquad E(0) \;=\; \begin{bmatrix} E_1 \\ E_2 \end{bmatrix} \qquad E(L) \;=\; \begin{bmatrix} E_3 \\ E_4 \end{bmatrix} \tag{1}$$

where the boundary conditions are also shown. The differential equations that describe the coupling of the waveguides [1] can be rewritten in a matrix form [2]

$$-\frac{i\partial}{\partial z}\begin{bmatrix} E_A(z) \\ E_B(z) \end{bmatrix} \;=\; \begin{bmatrix} \beta_A & 0 \\ 0 & \beta_B \end{bmatrix}\begin{bmatrix} E_A(z) \\ E_B(z) \end{bmatrix} \;+\; c\begin{bmatrix} 0 & 1 \\ 1 & 0 \end{bmatrix}\begin{bmatrix} E_A(z) \\ E_B(z) \end{bmatrix} \tag{2}$$

The first matrix describes the propagation in the two waveguides, where the β's are the propagation constants. The coupling between waveguide A and B is handled by the right-hand matrix, and has coupling coefficient c. It is convenient to write the differential equation in shorthand notation, the coefficients are incorporated into a matrix **K**

$$-\frac{i\partial}{\partial z}E(z) \;=\; (\beta\mathbf{I}+\mathbf{K})\,E(z) \qquad \text{where} \quad \mathbf{K} \;\equiv\; \begin{bmatrix} b & c \\ c & -b \end{bmatrix} \tag{3}$$

β is the average propagation constant, and b is half of the propagation constant difference

$$b \;\equiv\; (\beta_A-\beta_B)/2 \qquad \text{and} \qquad \beta \;\equiv\; (\beta_A+\beta_B)/2 \tag{4}$$

The differential equation (3) will have an exponential solution of the form

$$E(z) \;=\; e^{i\beta z}\,e^{i\mathbf{K}z}\,E(0) \;\equiv\; e^{i\beta z}\,\mathbf{A}\,E(0) \tag{5}$$

The first term is for the average phase shift $e^{i\beta z}$ in the coupler and will be dropped. The differential equation (3) will be explicitly solved when an explicit expression for $\mathbf{A} \equiv e^{i\mathbf{K}z}$ is found. $\mathbf{A}$ is a 2×2 matrix that describes the transfer function for the coupler, and is also called the coupler matrix. The exponential matrix can be computed by the method of diagonalization [3], by factoring $\mathbf{K}$ into a symmetric form

$$\mathbf{K} \;=\; \mathbf{QDQ^{-1}} \tag{6}$$

where $\mathbf{D}$ is a diagonal matrix containing the two eigenvalues Λ_1 and Λ_2 of $\mathbf{K}$, and $\mathbf{Q}$ is a matrix whose columns are the corresponding normalized eigenvectors X_1 and X_2 of $\mathbf{K}$. Consider the case of identical fibers; the eigenvalues are found to be $\Lambda_1 = +c$ and $\Lambda_2 = -c$,

$$\mathbf{D} \;=\; \begin{bmatrix} c & 0 \\ c & -c \end{bmatrix} \qquad \mathbf{Q} \;\equiv\; \frac{1}{\sqrt{2}}\begin{bmatrix} 1 & -1 \\ 1 & 1 \end{bmatrix} \qquad \mathbf{Q^{-1}} \;\equiv\; \frac{1}{\sqrt{2}}\begin{bmatrix} 1 & 1 \\ -1 & 1 \end{bmatrix} \tag{7}$$

The coupling matrix $\mathbf{A}$ is computed by calculating the exponential of the diagonal matrix

$$\mathbf{A} \;=\; e^{i(\mathbf{QDQ^{-1}})z} \;=\; \mathbf{Q}e^{i\mathbf{D}z}\mathbf{Q^{-1}} \;=\; \frac{1}{2}\begin{bmatrix} 1 & -1 \\ 1 & 1 \end{bmatrix}\begin{bmatrix} e^{icz} & 0 \\ 0 & e^{-icz} \end{bmatrix}\begin{bmatrix} 1 & 1 \\ -1 & 1 \end{bmatrix}$$

$$= \;\frac{1}{2}\begin{bmatrix} e^{icz}+e^{-icz} & e^{icz}-e^{-icz} \\ e^{icz}-e^{-icz} & e^{icz}+e^{-icz} \end{bmatrix} \;=\; \begin{bmatrix} \cos cz & i\sin cz \\ i\sin cz & \cos cz \end{bmatrix} \tag{8}$$

Equation (8) illustrates the periodic nature of the coupling process, and that the relative phase difference between the output fields is $\theta = +\pi/2$. For a coupler of length L, the variable $k \equiv \sin(cL)$ can be defined such that k^2 is the intensity splitting ratio of the device. Now the coupler matrix can be expressed in terms of a single parameter:

$$\mathbf{A} \;=\; \begin{bmatrix} \sqrt{1-k^2} & i\,k \\ i\,k & \sqrt{1-k^2} \end{bmatrix} \tag{9}$$

2. DIFFERENTIAL NORMAL MODE LOSSES (DNML) IN THE COUPLER

To incorporate differential normal mode losses, Equation (8) is rewritten to incorporate losses for the symmetric and antisymmetric supermodes [4]. The modified transfer function is called $\mathbf{A'}$, and ρ_s and ρ_a are the amplitude transmission coefficients for the symmetric and antisymmetric supermodes, respectively.

$$\mathbf{A'} = \frac{1}{2}\begin{bmatrix} \rho_s e^{icz} + \rho_a e^{-icz} & \rho_s e^{icz} - \rho_a e^{-icz} \\ \rho_s e^{icz} - \rho_a e^{-icz} & \rho_s e^{icz} + \rho_a e^{-icz} \end{bmatrix} \tag{10}$$

Average and differential transmission coefficients are now defined such that $\rho \equiv (\rho_s + \rho_a)/2$ and $\varepsilon \equiv (\rho_s - \rho_a)/2$ which permits calculating $\mathbf{A'}$ in terms of $\mathbf{A}$:

$$\mathbf{A'} = \begin{bmatrix} \rho\cos cz + i\varepsilon\sin cz & i\rho\sin cz + \varepsilon\cos cz \\ i\rho\sin cz + \varepsilon\cos cz & \rho\cos cz + i\varepsilon\sin cz \end{bmatrix} \equiv \mathbf{N \cdot A} \tag{11}$$

where $\mathbf{N}$ is a matrix that incorporates DNML by mixing the coefficients of the $\mathbf{A}$ matrix.

$$\mathbf{N} \equiv \begin{bmatrix} \rho & \varepsilon \\ \varepsilon & \rho \end{bmatrix} \tag{12}$$

For the case of finite DNML, the relative phase difference between the coupler outputs will be less than $\pi/2$; the deviation from the ideal case is found to be

$$\theta(k^2) - \frac{\pi}{2} = -\arctan\left(\frac{\varepsilon}{\rho}\frac{k}{\sqrt{1-k^2}}\right) - \arctan\left(\frac{\varepsilon}{\rho}\frac{\sqrt{1-k^2}}{k}\right) \tag{13}$$

The coupler transmission coefficient ρ is often assumed to be unity, and all of the resonator loss (coupler, splice, coil) is lumped in the fiber loss value. Figure 2 is a plot of the intensity and phase behavior of a coupler using the matrix methodology, with $c = 0.001$ per micron, and intensity I_0 launched into port 1. The two sinusoidal curves are the intensities leaving ports 3 and 4, illustrating the periodic coupling behavior. The DNML phase error for $\rho = 0.99$ and $\varepsilon = 0.01$ is shown in the third plot on Figure 2. Devices operating near $k^2 = 0.5$, the deviation from the ideal case is small, but this error becomes large for the type of couplers used in low-loss resonators.
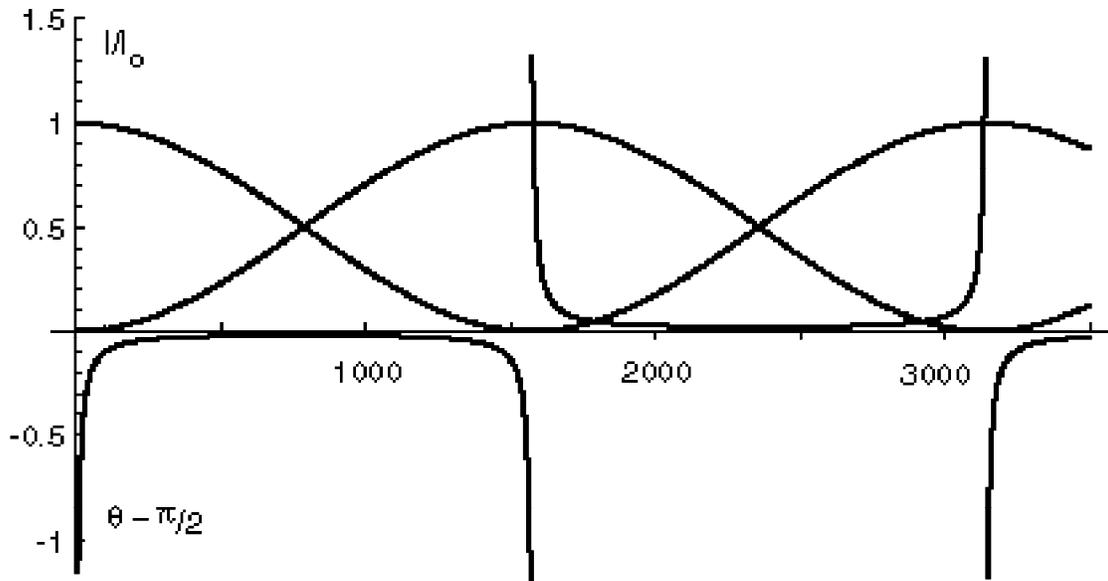

Figure 2. Phase Behavior with Differential Normal Mode losses.

For the resonator constructed out of a single coupler, deviation from the ideal $\pi/2$ phase shift will be exhibited as an asymmetric lineshape, and is a well-known source of errors in interferometric sensors [4]. Comparing, say a 1% coupler to a 90% coupler, one notes that the DNML phase error is equal for both cases. Indeed, $\theta(k^2) = \theta(1-k^2)$ for the first half of the coupling cycle 0 - 100%, and as z is increased $\theta(k^2) = -\theta(1-k^2)$ for the 100 - 0% region. All other factors being equal, there seems to be no advantage from the DNML viewpoint for a low or high splitting ratio coupler. For resonators made from a single coupler, the DFR and CFR cavity topology are equally affected by nonzero ε values. The effect of DNML is reciprocal, however for FM heterodyne signal processing [5], electronics phase delay will tend to imbalance the reciprocal null offset induced by DNML.

3. RESONATOR ANALYSIS

Consider the two single-coupler resonators which are shown in Figure 3; they are comprised of two devices: a 4-port coupler, and a length of fiber. The devices can be modeled as a six-port system, and two connection topologies are possible, using a low or a high splitting ratio coupler. Using the terminology of [6], the left-hand ring is a direct-coupled fiber resonator (DFR) with a closed loop, and the right-hand ring is a cross-coupled fiber resonator (CFR). The two topologies will now be examined and compared.
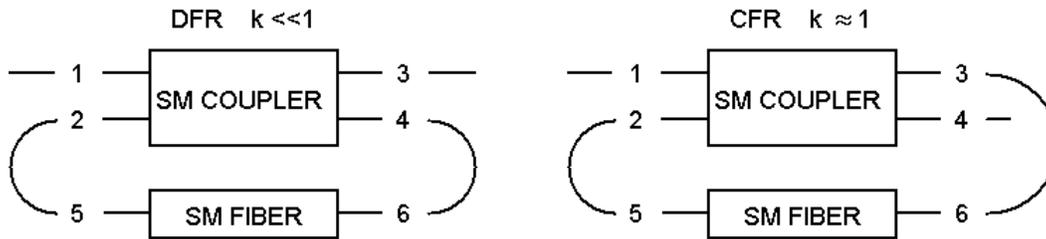

Figure 3. DFR and CFR Topology Examples.

The scattering matrix formalism will enable the separation of device and topology characteristics. A 6×6 scattering matrix **S** can be defined to represent the fiber and coupler, which relates the six fields exiting the devices to the six fields entering the devices:

$$E_{out} = \mathbf{S}\, E_{in} \tag{14}$$

The S-matrix can be assembled out of the 2×2 coupler matrix **A** or **A'**, and a second 2×2 scattering matrix **F**, which describes the optical characteristics of the fiber. For the case of no device backscattering, the submatrix **0** is a 2×2 matrix containing all zeroes.

$$\mathbf{S} \equiv \begin{bmatrix} [\mathbf{0}] & [\mathbf{A}^{\mathrm{T}}] & [\mathbf{0}] \\ [\mathbf{A}] & [\mathbf{0}] & [\mathbf{0}] \\ [\mathbf{0}] & [\mathbf{0}] & [\mathbf{F}] \end{bmatrix} \qquad \text{and} \qquad \mathbf{F} \equiv \begin{bmatrix} 0 & \rho\, e^{i\phi} \\ \rho\, e^{i\phi} & 0 \end{bmatrix} \tag{15}$$

The $\rho\, e^{i\phi}$ coefficients accounts for the propagation down the fiber by giving E_5 as a function of E_6, and vice versa. ρ is now the lumped transmission coefficient for the resonator, and ϕ is the round-trip phase shift in the cavity. The S-matrix defines all of the inputs and outputs for the devices and is general, e.g. backscattering components are located on the diagonal of **S**. The topology of the system is represented by a geometry matrix **G [7]**

$$E_{in} = \mathbf{G}\, E_{out} + E_o \tag{16}$$

G yields the fields entering the devices as a function of the fields exiting the devices, which is topology-dependent. The initial conditions are a monochromatic source connected to port 1, and is a $6{\times}1$ column vector $E_o = [1 \ 0 \ 0 \ 0 \ 0 \ 0]^T$. The G-matrices for the two topology types can be written from inspection of Figure 3:

$$
\mathbf{G}_{DFR} \equiv
\begin{bmatrix}
0 & 0 & 0 & 0 & 0 & 0 \\
0 & 0 & 0 & 0 & 1 & 0 \\
0 & 0 & 0 & 0 & 0 & 0 \\
0 & 0 & 0 & 0 & 0 & 1 \\
0 & 1 & 0 & 0 & 0 & 0 \\
0 & 0 & 0 & 1 & 0 & 0
\end{bmatrix}
\quad \text{and} \quad
\mathbf{G}_{CFR} \equiv
\begin{bmatrix}
0 & 0 & 0 & 0 & 0 & 0 \\
0 & 0 & 0 & 0 & 1 & 0 \\
0 & 0 & 0 & 0 & 0 & 1 \\
0 & 0 & 0 & 0 & 0 & 0 \\
0 & 1 & 0 & 0 & 0 & 0 \\
0 & 0 & 1 & 0 & 0 & 0
\end{bmatrix}
\tag{17}
$$

Since **S** is not singular, the inverse of Equation (14) can be computed and substituted into equation (16), and the E_{in} variable can be eliminated:

$$
E_{in} \ = \ \mathbf{S}^{-1} \ E_{out} \tag{18}
$$

$$
E_{in} \ = \ \mathbf{G} \ E_{out} \ + \ E_o \ = \ \mathbf{S}^{-1} \ E_{out} \tag{19}
$$

$$
\Rightarrow \quad E_o \ = \ (\mathbf{S}^{-1} - \mathbf{G}) \ E_{out} \tag{20}
$$

Equation (20) is now inverted, solving for the output fields as a function of the initial conditions. This task and subsequent plotting is considerably simplified by symbolic algebra packages such as Mathematica. To compare the two topologies, use the following identities for the field leaving the coupler:

$$
E_{DFR} \ = \ E_{out}(\text{port 3}) \ = \ (\mathbf{S}^{-1} - \mathbf{G}_{DFR})^{-1} \ E_o \tag{21}
$$

$$
E_{CFR} \ = \ E_{out}(\text{port 4}) \ = \ (\mathbf{S}^{-1} - \mathbf{G}_{CFR})^{-1} \ E_o \tag{22}
$$

4. SPLITTING RATIO TOLERANCE

The result of Equation (22) is an equation which describes the classic Fabry-Perot interferometer operated in a reflection-mode, i.e., is nearly unity off-resonance with periodic resonant nulls. For the DFR with $k^2 \ll 1$, the output field leaving port 3 of the coupler is given by

$$
E_{DFR} \ = \ \frac{(2-k^2)x \ - \ \sqrt{1-k^2} \ (1+x^2)}{-x^2(1-k^2) \ + \ 2x\sqrt{1-k^2} \ - \ 1} \qquad \text{where} \quad x \equiv \rho \ e^{i\phi} \tag{23}
$$

For the case of the CFR, the splitting ratio k^2 is close to 100%, and the output field is

$$
E_{CFR} \ = \ \frac{(1+k^2)x \ + \ ik \ (1-x^2)}{-k^2 x^2 \ - \ 2ikx \ + \ 1} \tag{24}
$$

To permit comparison of the DFR and CFR, the parameter κ^2 is introduced that is the splitting ratio offset from the 100% value. Substituting $k^2 \equiv 1 - \kappa^2$ into the previous result, redefining $x + \rho \ e^{i(\phi - \pi/2)}$, and multiplying by $e^{-i\pi/2}$ will result an equation identical to Equation (23)

$$E_{CFR} = \frac{(2-\kappa^2)x - \sqrt{1-\kappa^2}\,(1+x^2)}{-x^2(1-\kappa^2) + 2x\sqrt{1-\kappa^2} - 1} \tag{25}$$

The behavior of a DFR with splitting ratio k^2 will be the same as for an equivalent CFR having an equal κ^2 value. The finesse F and dip depth are strong functions of the resonator losses and the coupler splitting ratio [8]. Figure 3 illustrates the dip depth and finesse characteristics as a function of splitting ratio for different loss values.
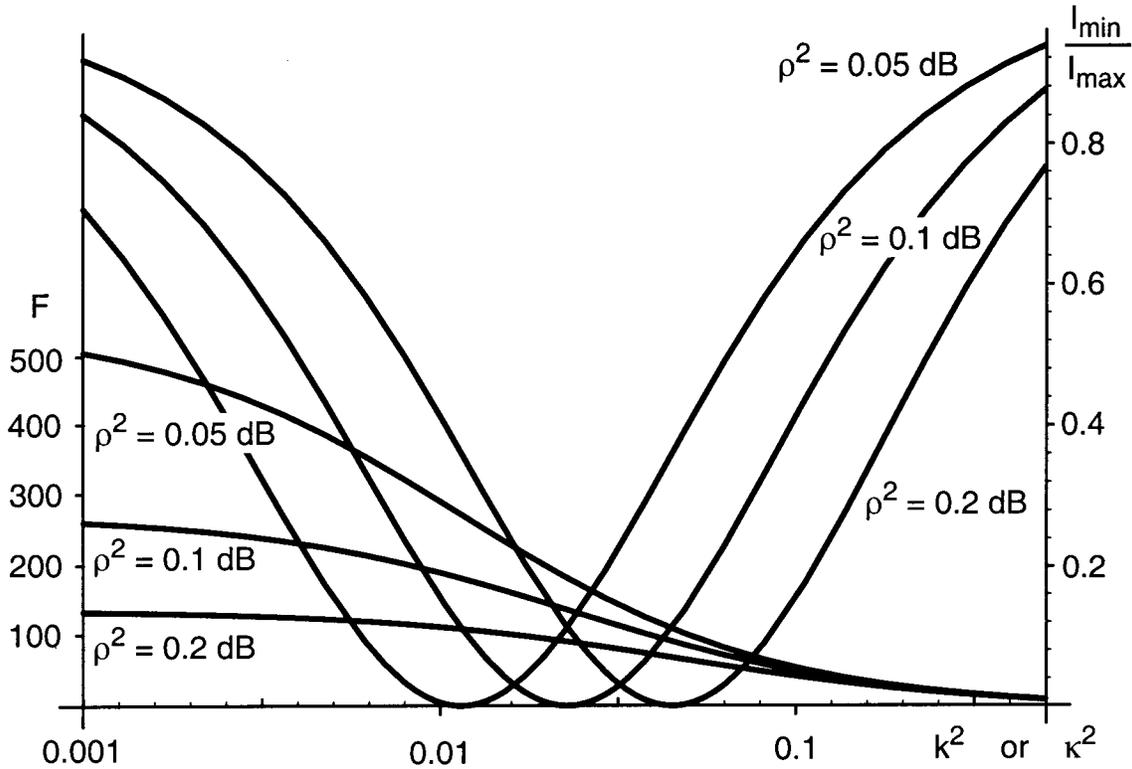

Figure 4. Finesse and Minimum Dip Intensity as a Function of Splitting Ratio.

Resonator for RFOG and other applications have resonator performance that is bounded by a worst-case I_{min}/I_{max} value, to minimize shot noise at the photodetector. There is also minimum and maximum finesse requirements, usually set by system requirements and electronics limitations. If the assembly loss can be predicted with confidence, the above type of plot is useful to determine acceptable splitting ratios for a given loss range. For example, consider a resonator with a performance requirement of finesse $F > 50$ and dip depth $I_{min}/I_{max} < 10\%$. For a DFR made with total loss between 0.1 and 0.2 dB, a coupler with splitting ratio $2.25\% < k^2 < 4\%$ will be sufficient to meet the specifications. In the case of a CFR, the range would be $96\% < k^2 < 97.75\%$ to achieve the same resonator performance levels.

5. POLARIZATION

The polarization characteristics of the coupler is modeled by expanding the formalism to account for the two polarization eigenstates of the optical fiber. The details of the calculations are reported separately [9] and an example of the model is presented. Figure 5 is a plot of the polarization extinction ratio as a function of splitting ratio, for the case of fiber principal axes misaligned by 5 degrees. The fiber is assumed to have a beat length of 2 mm and the coupling coefficient is still 0.001 per micron.

It seems that the high-splitting ratio devices will suffer worse polarization cross-coupling than for a low-splitting ratio coupler. This is because that for the case of misaligned principal axes, the orthogonal polarization is coupled in a distributed

manner and results in large polarization cross-coupling values. In this context, the DFR is superior to the CFR, all other things remaining equal.
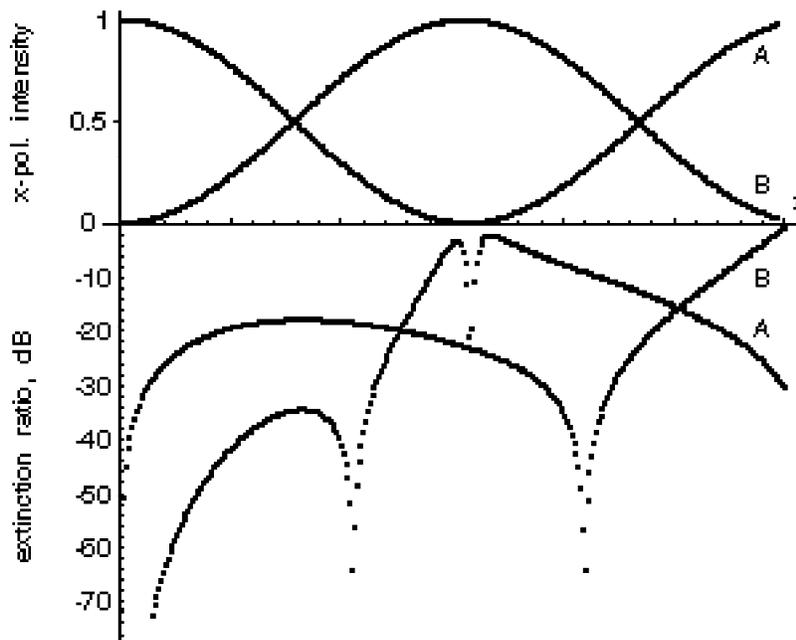

Figure 5. Polarization Behavior of PM Coupler.

The impact of polarization cross-coupling on the reciprocity of a ring resonator has been discussed in reference 2, where the high splitting ratio case was considered in detail. Those results agree with Figure 5 in that the high splitting ratio cross-talk is on the order of the misalignment angle between the A and B fibers in the coupler. The error propagation mechanism at work in rings with both high- and low-splitting ratio couplers is that a residual, unextinguished y-polarization from the laser enters the ring-coupler and cross-couples back into the primary signal channel, which is the x-polarization channel. The phase and amplitude noise from this interference causes unwanted noise in the output of the resonator. However the polarization cross-coupling in the weak coupling case is substantially smaller than the strong coupling case. Therefore the effect of signal contamination should be smaller by perhaps another -20 dB as suggested by Figure 5.

Now refer to the single coupler resonators as resonance absorption rings (RAR) to distinguish them from the resonance transmission rings (RTR) in which there are 2 couplers and the output is a resonance peak instead of a resonance dip. These latter RTR will also benefit from the low splitting ratio couplers. However, it can be shown that the RTR configuration has, as one of its dominant polarization cross-coupling interference terms, a term from the primary signal channel cross-coupled through the first RTR coupler and cross-coupled again through the second RTR coupler before recirculating in the ring. Therefore any polarization filtering prior to insertion of light into the ring is of no avail. The phases of interference errors generated in this way are non-reciprocal. It is imperative to use the weak coupling case for gyros in the RTR configuration, since the interference amplitude is proportional to the product of A & B extinction ratios. Furthermore a very low coupling ratio is desired to minimize the relative polarization cross coupling.

6. COHERENT BACKSCATTER IN RESONATORS

The ring is modeled as a fiber-optic resonant absorber with a single high splitting ratio coupler in a fiber loop of length L. Each incremental length, dz, of fiber acts as a backscattering source i s(z) dz, which is proportional to the amplitude at z, E exp $\{-2\pi i(\upsilon t - z/\lambda)\}$, and where E is given in Equation (24). The incremental guided wave reflected from the interval dz is defined at z as iEs(z) exp$\{-2\pi i(\upsilon t + z/\lambda)\}$ dz.

Although s(z) is a random function locally it is periodic globally from ring closure: s(z + L) = s(z). Consequently it can be written as a Fourier series

$$s(z) \quad = \quad \sum_{p=-\infty}^{\infty} S(p) \, e^{2\pi p i z / L} \tag{26}$$

The scattered wave back at the coupler origin, z = 0, is proportional to the sinc factor $\dfrac{\sin \pi(p - 2L/\lambda)}{\pi(p - 2L/\lambda)}$, which behaves as a delta function centered at p = 2L/λ. This implies that the spatial frequency component S(2L/λ) strongly dominates backscatter of wavelength λ, which is well known in the case of gratings. The physical interpretation of the sinc factor is that the coherent backscatter amplitude coupled out of the ring comes from the coherent sum of each of the 2L/λ half-wave segments in the fiber ring.

At a ring resonance where 2L/λ is an exact integer, the relative size of the backscatter is just LS(2L/λ), which is a random function for each fiber.

Let us illustrate the statistical nature of the coefficient s(z) by considering many point-like scattering sites randomly distributed along a 10-m fiber. These scatterers are each located at the random points z_n and we can assume the weights to be random. Integration of the scattered wave is then a finite, but large sum of N random coefficients, s_n, randomly distributed at z_n, each with $4\pi z_n/\lambda$ out and back phase delay.

In Figure 6 is a graph of the amplitude and phase of each wavelet scattered back to the fiber coupler for a random distribution of 5723 scatterers along a 10-m fiber. Each point represents one of the N amplitudes. The scattering amplitude is the vector sum of all these points, which is a random walk in two dimensions. Figure 7 illustrates the dependence of the backscattered amplitude on the nonuniform stretching of the fiber by up to 10 wavelengths. Uniform stretching at resonance would only make
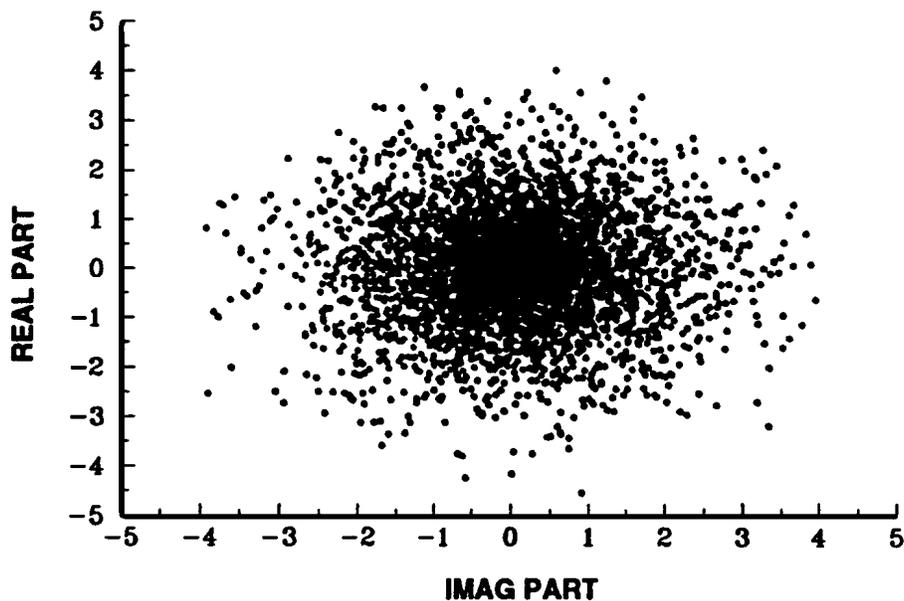

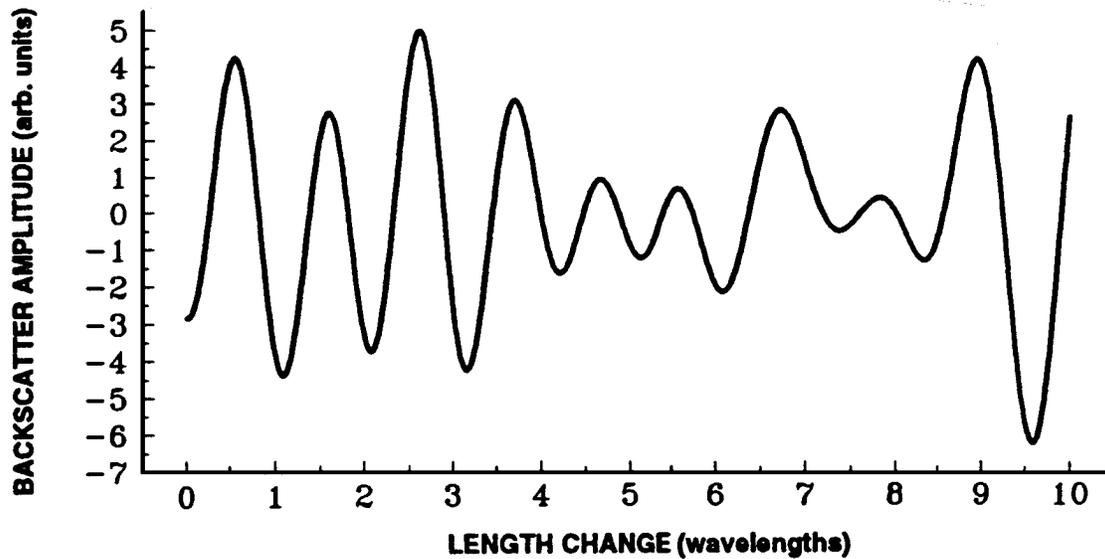Figure 6. Phase and amplitude of simulated scattering sites.

Figure 7. Phase and amplitude of simulated scattering sites.

λ change in proportion to L and $S(2L/\lambda)$ would be constant. The ordinate is the integrated backscatter amplitude. The abscissa is the fiber length change in wavelengths. The scale is arbitrary, but the dependence on length exhibits the kind of structure seen in coherent backscatter. With from 3 up to 131,071 random points, the scale goes roughly as the square root of this number, and the characteristic random waviness of the amplitude versus non-uniform stretching does not depend on the number of scatterers.

7. SUMMARY

Table 1 summarizes the characteristics of the DFR and CFR cavity topologies; only the CFR can be fabricated as a spliceless assembly. The DFR requires at least one splice in the cavity, however low-loss passive PM fiber splicing techniques [11] have minimized this impact. In fact, the splice can become the key to some polarization-error reduction schemes [12].

Table 1. Summary of DFR versus CFR comparison.

	assembly	asymmetry	k^2, κ^2 tolerance	PM coupler polarization	resonator backscatter
DFR $k^2 \ll 1$	Must be spliced	no difference	no difference	better	no difference
CFR $k^2 \approx 1$	Spliced or spliceless			worse	

In conclusion, it seems that the DFR is the preferred configuration for single-coupler resonators. By using a low-SR coupler, the effects of polarization degradation in the coupler fabrication process can be reduced. One drawback of the DFR is that splice loss can limit the ultimate finesse achievable, but the RFOG servoelectronics has difficulty in acquiring and locking to dips with F >> 100. There seems to be no theoretical advantage of either DFR or CFR topology with respect to asymmetry effects, SR tolerance, and backscatter effects.

One practical implication is that fabrication of high-quality polished and fused PM couplers is easier for low-SR values [13]. The fused coupler for a DFR would have a larger taper waist, and experience has shown that there is better yield, ruggedness, and reliability for low-SR couplers. It is also easier to control the splitting ratio during fabrication, as coupling commences somewhat slower during the initial stages of the tapering process. Qualitatively, better polarization performance is

observed experimentally for low-SR couplers; it would be desirable to verify the above model by measuring the SOP during the tapering process.

8. REFERENCES

1.   D. Marcuse, "The coupling of degenerate modes in two parallel dielectric waveguides," Bell Systems Technical Journal, Vol. 50, No. 6, pg. 1791-1816 (1971).

2.   R. Carroll, "Polarization crosstalk in a PM fiber resonator gyro," Fiber Optic and Laser Sensors VII, SPIE Vol. 1169, pg. 388-399 (Boston, 1989).

3.   G. Strang, Linear Algebra and its Applications, Harcourt Brace Jovanovitch (1988).

4.   R.C. Youngquist, L.F. Stokes, and H.J. Shaw, "Effects of normal mode loss in dielectric waveguide directional couplers and interferometers," IEEE Journal of Quantum Electronics, Vol. 19, No. 12, pg. 1888-1896 (1983).

5.   R. Carroll, C.D. Coccoli, D. Cardarelli, and G.T. Coate, "The passive resonator fiber optic gyro and comparison to the interferometer fiber gyro," Fiber Optic Gyros: 10th Anniversary Conference, Proc. SPIE Vol. 719, pg. 169-177 (Cambridge, Mass., 1986).

6.   F. Zhang and J.W. Lit, "Direct-coupling single-mode fiber ring resonator," Journal of the Optical Society of America, Vol. 5, No. 8, pg. 1347-1355 (1988).

7.   F. Sanchez, "Matrix algebra for all-fiber optical resonators," IEEE Journal of Lightwave Technology, Vol. 9, No. 7, pg. 838-844 (1991).

8.   Y. Ohtsuka and Y. Imai, "Performance analysis of an all-fiber resonant-ring interferometric sensor," Applied Optics, Vol. 24, No. 33, pg. 4199-4205 (1985).

9.   R.P. Dahlgren, "Studies in Fiber-Optic Couplers and Resonators," Massachusetts Institute of Technology S.M. Thesis (1993).

10.   R. Carroll, "Backscatter and resonant fiber-optic gyro scale factor," IEEE Journal of Lightwave Technology, Vol. 7, No. 12, pg. 1895-1900 (1989).

11.   H. Taya, K. Ito, T. Yamada, and M. Yoshinuma, "New splicing method for polarization-maintaining fibers," OFC'89, Optical Society of America pg. 164-165 (Houston, 1989).

12.   G.A. Sanders, R.B. Smith, and G.F. Rouse, "Novel polarization-rotating fiber resonator for rotation sensing applications," Fiber Optic and Laser Sensors VII, Proc. SPIE Vol. 1169, pg. 373-381 (Boston, 1989).

13.   Y. Anjan, Honeywell, Inc., personal communications.